Journal of Nuclear Materials 385 (2009) 329–333

Contents lists available at ScienceDirect

Journal of Nuclear Materials

journal homepage: www.elsevier.com/locate/jnucmat

Deformation and microstructure of neutron irradiated stainless steels with different stacking fault energy

Xiaoqiang Li *, A. Almazouzi

SCK·CE, Nuclear Materials Sciences Institute, LHMA, Boeretang 200, 2400 Mol, Belgium

ARTICLE INFO

PACS:
61.82.Bg
61.80.Hg
61.67.Nn
68.37.Lp
62.20.Fe

ABSTRACT

The influence of the stacking fault energy (SFE) on the microstructure, mechanical property and deformation behaviour of stainless steels before and after irradiation was investigated. The mechanical properties, such as strength, ductility, strain hardening and irradiation induced hardening behaviours of 3 alloys with various SFEs are quite different. Such significant variations of mechanical properties must result from the different microstructures, deformation mechanisms and defects accumulation behaviours. Thus, the microstructures, deformation mechanisms and irradiation induced small defect clusters (including their types, natures, densities and size distributions) of 3 alloys are determined in detail by transmission electron microscopy. It indicated that before irradiation, alloy with low SFE has more localised deformation behaviour than alloy with high SFE. After irradiation, in the samples with low SFE, the irradiation induced stacking fault tetrahedral was observed, while in the ones with high SFE, the dominant defects are Frank loops. All the results shown that, SFE has a strong effect on both the deformation mechanism and irradiation induced defect accumulation behaviour of stainless steels.

1. Introduction

It is well established that the irradiation induced microstructrual and microchemical changes in austenitic alloys may affect the irradiation-assisted stress corrosion (IASCC) susceptibility, where irradiation modifies the response of a material to both mechanical loading and environmental interaction [1]. Current knowledge highlights the Radiation Induced Segregation (RIS) [2] and the Radiation Hardening [3] as the two main effects on the IASCC.

Stacking fault energy (SFE) may have strong effect on IASCC susceptibility of austenitic stainless steels because it plays an important role in every process of localised plastic deformation, work hardening and creep behaviour [4]. Since SFE influences the plastic flow and neutron irradiation induced defects accumulation behaviour of the material, the study of the impact of SFE variations on the deformation mode and stress corrosion cracking (SCC) behaviour of irradiated and unirradiated austenitic steels is important to the understanding of IASCC mechanism.

The aims of this work, as a task within the European Project PERFECT, are to investigate the influence of the SFE on the deformation mechanisms, mechanical properties, neutron irradiation induced defects accumulation and IASCC susceptibility of stainless steels. In order to achieve this goal, three model stainless steels were fabricated with different SFEs by controlling their chemical compositions especially the contents of C, N, Ni and Si. A systematic study is performed on these materials to examine the potential impact of SFE on the microstructure, mechanical properties, deformation modes and neutron irradiation induced defect accumulation behaviour using TEM analysis and tensile testing.

2. Experimental

Using high purity starting elements, three stainless steels have been fabricated under highly controlled conditions. Then hot and cold rolled to reach the desired plate thickness and subsequently solution annealed to obtain a homogeneous microstructure. All the plates were analysed chemically and metallographically to check their homogeneity.

The SFEs of the 3 alloys were measured experimentally by TEM applying both partial dislocations splitting and dislocation node methods [5]. The dependence of SFE on the composition implies a chemical interaction between the solute atoms and the stacking fault so that the SFE can be changed apparently by changing the concentrations of the elements of C, N, and Si. The compositions and measured SFE values are listed in Table 1. Based on their SFEs, the 3 alloys are called LSFE, Ref SFE and HSFE for the low, medium and high SFE, respectively.

Standard tensile tests were performed at a constant nominal strain rate of $3 \times 10^{-4}\,s^{-1}$ and at temperature ranging from 123 to 573 K. After tensile tests, discs from the deformed (2–10%) or

* Corresponding author. Tel.: +32 14 33 31 91; fax: +32 14 32 12 16.
E-mail address: xiaoqiang.li@sckcen.be (X. Li).

0022-3115/$ - see front matter © 2008 Elsevier B.V. All rights reserved.
doi:10.1016/j.jnucmat.2008.12.008

Table 1
The chemical compositions and the SFEs of the 3 model alloys.

Alloys	C	N	Si	P	S	Cr	Mn	Ni	E_{SF} (mJ m^{-2})
LSFE	0.04	0.06	1.07	0.033	0.02	18.04	1.52	8.75	11
Ref SFE	0.05	0.023	0.44	0.033	0.02	17.64	1.56	8.6	31
HSFE	0.07	0.032	0.1	0.035	0.043	18.63	1.59	16.23	46

fractured test were cut along 45° with respect to the tensile axis and polished for the TEM observation.

The specimens were irradiated in the CALLISTO rig of the Belgian material test reactor (BR2) at a temperature of about 573 ± 5 K. Fe activation dosimeters were used for the determination of the fast neutron flux and fluence. The neutron flux was about 7.51×10^{13} (cm^{-2} s^{-1}), the fluence was 5.27×10^{20} (cm^{-2}) and the damage dose was estimated to be of about 0.9 displacements per atom (dpa) [6].

The irradiated TEM specimens were mechanically and electrochemically polished in a hot cell. Neutron irradiation induced defects in the specimen are imaged by the diffraction contrast arising from their elastic strain fields. In order to obtain strain contrast images from the various types of defects under optimum experimental conditions, it is necessary to tilt the specimen obtaining a succession of two beam and weak beam conditions, tilt through a large angle (~30°) maintaining specific reflection conditions, and tilt from one known specimen orientation to another. Thus, only by a careful comparison of several different micrographs taken under different diffraction conditions, a complete picture of the microstructure could be built up [7].

3. Results

3.1. Microstructures as the received state

The as received samples were observed by TEM. As demonstrated in Fig. 1, in crystals with an fcc structure, the {1 1 1} type stacking faults are formed when a gliding dislocation with a Burgers vector $a/2\langle 1\,1\,0\rangle$ (where, a is the lattice parameter) actually dissociated into two partial dislocations with Burgers vector $a/6\langle 1\,1\,2\rangle$, separated by a stacking fault. This separation increases with decreasing SFE [8], which makes cross-slip difficult. Therefore, for the low SFE alloy, because the separation of two partial dislocations is large, the gliding dislocations are confined to a thin slip band and show a banded, linear array dislocation microstructure. This planar dislocations slip can easily form twins and induces martensitic transformation. While in high SFE alloy, this separation is small, the cross-slipping and climbing of partial dislocations becomes easier and the mobile dislocations become tangled and arranged in cells.

3.2. Tensile properties

Fig. 2 illustrates the mechanical properties of the three alloys as function of temperature and shows strong temperature dependencies of strength and ductility. The strength increases when test temperature decreases, but the ductility did not decline systematically with decreasing temperature. The ductility of the LSFE and Ref SFE alloys shows a maximum at room temperature while the ductility of the HSFE alloy increased monotonously with decreasing temperature from 573 to 123 K. This inverse elongation behaviour of the HSFE alloy is similar to the low temperature behaviour of the austenitic high manganese steels, the so-called TRIP steel [9]. It is due to earlier necking at higher temperatures and delayed necking at lower temperatures since the deformation mechanism changed when the temperature decreases. Above 573 K, the flow behaviours of 3 alloys are almost the same. While below room temperature, the LSFE and Ref SFE alloys show two-stages of hardening, similar to what has been observed in other austenitic steels [10] used for non nuclear applications. The HSFE alloy does not show this behaviour in the test temperature range considered here. More detailed analysis will be published elsewhere.

3.3. Deformation mechanisms

Significant variations of hardening behaviour must result from the deformation mechanism change. TEM observation of tensile deformed samples at each temperature gives a reasonable explanation of the observed trends in mechanical behaviour. To illustrate the main difference of the flow behaviours which was observed below room temperature, the microstructure of the deformed samples below 223 K is illustrated in Fig. 3. It is shown that strain-induced martensitic transformation happens in the LSFE and Ref SFE alloys while only twins were observed in HSFE alloy. Twinning and martensitic transformation are the predominant deformation mechanisms of the LSFE and Ref SFE alloys, while dislocation glide and twinning are the main plasticity mechanisms of the HSFE alloy below room temperature [11]. For the LSFE and Ref SFE alloys, from 223 to 123 K, in the low strain region, twinning prevents necking, which leads to a pronounced improvement of ductility, while in the high strain region (>15%), strain-induced martensitic transformation occurs which enhanced strongly the

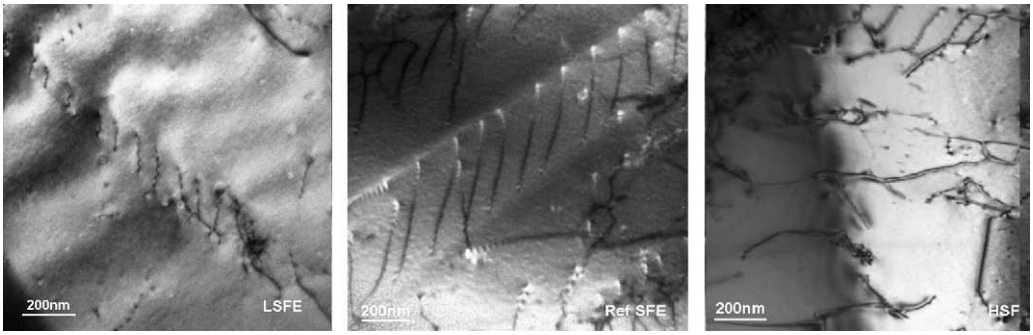

Fig. 1. Microstructure of the as received alloys showing that in low SFE alloy, dislocations are linearly arranged in the slip planes, while in the high SFE alloy, dislocation are tangled forming a cell structure.

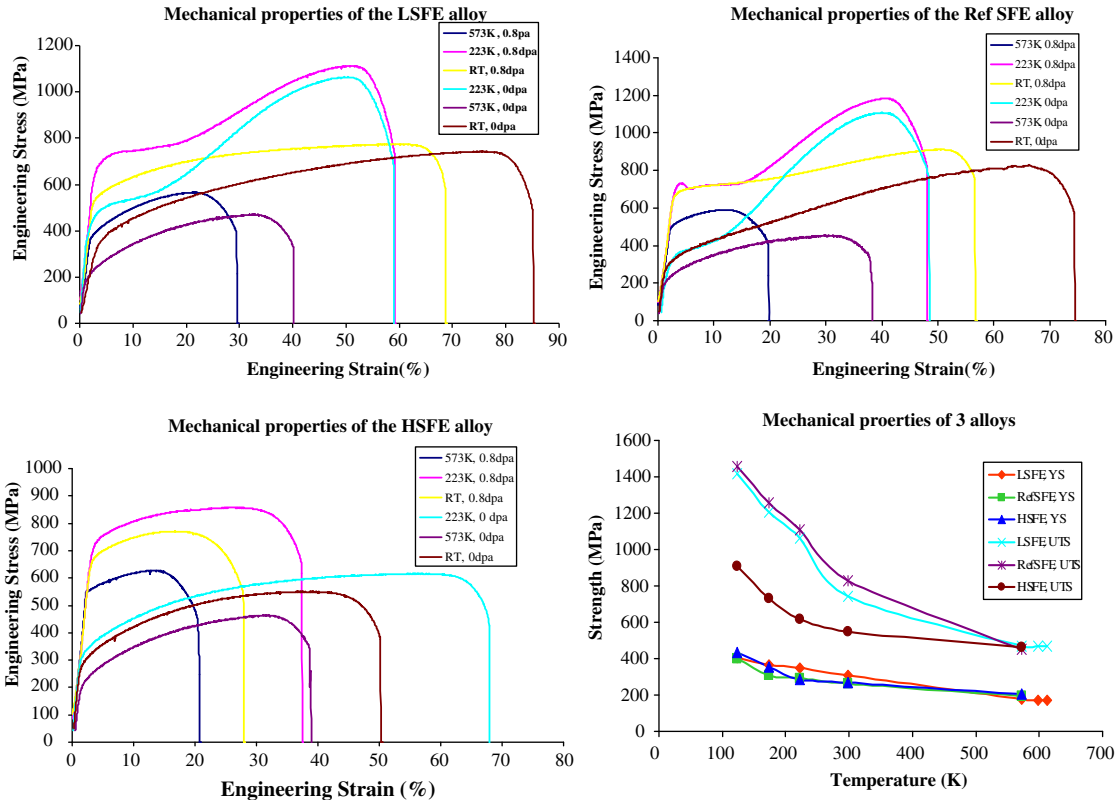

Fig. 2. Mechanical e properties of the 3 alloys with various SFE at different temperature.

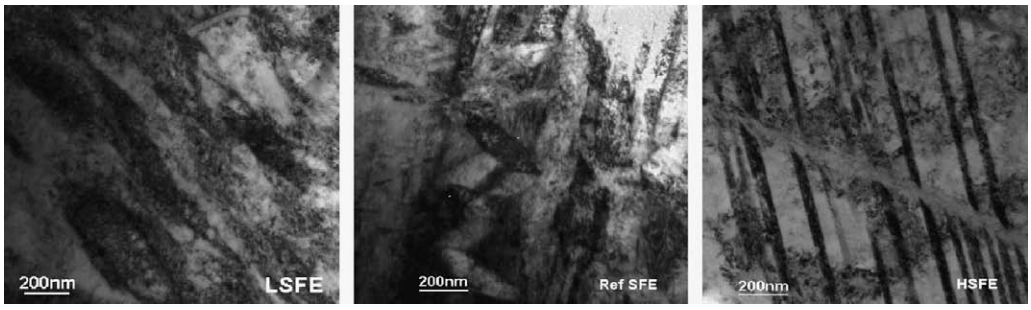

Fig. 3. Deformation microstructures of the 3 alloys deformed to 40% at 173 K, zone axis ([0 1 1]), showing strain-induced martensitic transformation in LSFE and Ref SFE alloys, while only twinning was observed in the HSFE alloy.

work hardening and reduced the ductility. Thus two-stage hardening behaviour is observed. For the HSFE alloy, dislocation glide and twinning are the dominating strain mechanisms. Twinning induced plasticity prevents material necking and leads to a pronounced improvement of ductility with a little strength, both strength and ductility increase monotonously with decreasing temperature. These results are similar to those observed in the high strength austenitic (Fe, Mn, Cr) steels [12] for instance. Above the 573 K, because the predominant deformation mechanism of 3 alloys is dislocation glide, therefore the mechanical properties of 3 alloys are almost the same.

3.4. Microstructure after irradiation

The flow behaviour (shape of strain–stress curves) of irradiated alloys is similar to the one observed in the unirradiated state when tested at the same temperature, but the irradiation induced hardening appears quite different in each of the investigated alloys (see Fig. 2). This must result from the differences of the irradiation induced defect accumulation behaviour in each of the alloys. Dark field TEM images (Fig. 4) show that, after irradiation, the microstructure of the LSFE alloy is quite inhomogeneous. There are some sets of stacking faults, edge-on micro-twins, high density small defect clusters, black dots, cell structure dislocations and dislocation pile ups near the grain boundaries. Some dislocations were pinned by defect clusters, which show that they interact with each other. LSFE alloy has such an inhomogeneous microstructure because of the fact that small defect clusters are obstacles to the planar dislocation glide and the climb, and the cross glide of the planar dislocation are hindered. In the Ref SFE alloy, the microstructure has sets of the thin-long stacking faults and edge-on micro-twins. Compared to the LSFE alloy, the distribution of the small defect clusters is more homogenous. In the irradiated HSFE alloy, high density defect clusters and dislocation cell structure as well as black dots are observed, but no stacking faults or micro-twins happened. Dislocations are pinned by small defect clusters and tangle

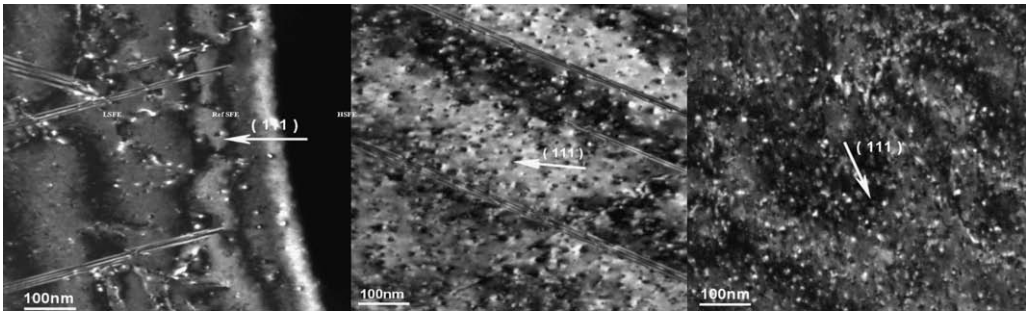

Fig. 4. Microstructures of the 3 irradiated alloys using the dark field weak beam imaging technique, showing sets of stacking faults, edge-on micro-twins, high density of small defect clusters in the LSFE and Ref SFE alloys and tangled dislocations in HSFE alloy in addition.

with other dislocations, and then the dislocation cell structures are formed. The structure of HSFE alloy is more homogeneous than that of the LSFE and Ref SFE alloys.

For the small defects clusters, the main difference is that the stacking fault tetrahedrons (SFTs) were observed in the LSFE and Ref SFE alloys but were not observed in the HSFE alloy. The dislocation loops are determined as Frank loops including both vacancy and interstitial types [6]. Since the whole irradiation induced hardening including both SFTs and dislocation loops induced hardening, the irradiation induced hardening is therefore different [6]. Irradiation induced deformation modes of the alloys at different temperatures were also studied in details and will be reported elsewhere. Important to notice at this stage is that the irradiation induced dislocation channelling was observed clearly in both LSFE and Ref SFE alloys despite the low irradiation dose [6].

3.5. Sizes and densities of the defect loops

The statistical evaluation of sizes and densities of the defect loops was carried out on several micrographs imaged at the same area under different diffraction vectors and deviation parameter *s*. Foil thickness were measured by recording at the same time one or more convergent beam patterns from thicker region of the foil [6,7]. The average sizes and densities of the defect loops by fitting of a Gaussian distribution to the experimental results are listed separately in Tables 2 and 3. It is shown that the effect of SFE on the irradiation induced defects accumulation behaviour is more likely to be linked to the type, nature and density of the small defect clusters [6].

Further investigations (not detailed in this paper) show that the dislocation channelling deformation mechanism could be observed in the irradiated LSFE and Ref SFE alloys but not in the HSFE one. It is thus expected that the low SFE alloys should be more susceptible to cracking when in contact with pressurised water (the work is on going). All these results show that SFE do have a non negligible effect on the irradiation induced defect accumulation behaviour of stainless steels.

Table 2
Average sizes of dislocation loops and stacking fault tetrahedrons.

Alloys	LSFE	Ref SFE	HSFE
Average loops size (nm)	6.11 ± 0.17	6.95 ± 0.14	5.73 ± 0.16
Average SFT size (nm)	6.34 ± 0.07	7.01 ± 0.09	

Table 3
Statistic results of the dislocation loops and SFTs densities.

Alloys	LSFE	Ref SFE	HSFE
Loops densities (m^{-3})	$(1.3 \pm 0.6) \times 10^{22}$	$(3.5 \pm 0.4) \times 10^{22}$	$(4.0 \pm 0.2) \times 10^{22}$
SFT densities (m^{-3})	$\sim(0.26 \pm 0.05) \times 10^{22}$	$\sim(0.30 \pm 0.07) \times 10^{22}$	

4. Conclusion

The effect of SFE on the microstructure and deformation behaviour was investigated using three austenitic stainless steels that were tensile tested in the temperature range from 123 to 573 K and irradiated in a fast reactor (BR2) to 0.9 dpa at 573 K. The results described in this paper allow drawing the following conclusions:

SFE affects the pattern of the glide dislocations arrangement in the slip planes, as expected:

(a) Lower SFE alloy has a linear banded dislocation microstructure, which can form twins and induces Martensitic transformation.
(b) Higher SFE alloy has a tangled celled dislocation microstructure.

After irradiation, in the low SFE alloy, the microstructure consists of black dots, stacking faults, edge-on micro-twins, dislocation loops and SFTs. Cell structure dislocations and linear dislocation pile ups were also observed near the grain boundaries. For the irradiated Ref SFE alloy, the microstructure is similar to the LSFE alloy except the density of the stacking fault which appears to be lower. For the irradiated HSFE alloy, only a higher density of black dot and lower content of defect loops were observed.

Acknowledgements

This work is partly supported by the FP6-European Project PERFECT with contract number F160-CT-2003-5088-40. The authors also would like to acknowledge the Nuclear Materials Science Institute of SCK·CEN, Belgium, and especially the microstructure analysis and mechanical test groups for their contribution. Many thanks also to Dr, S. van Dyck for his continuous interest and support.

References

[1] E.A. Kenik, R.H. Jones, G.E.C. Bell, IASCC, J. Nucl. Mater. 212–215 (1994) 52.
[2] J.T. Busby, G.S. Was, E.A. Kenik, J. Nucl. Mater. 300 (2002) 198.
[3] S.M. Brummer, E.P. Simonen, P.M. Scott, P.L. Andresen, G.S. Was, J.L. Nelson, J. Nucl. Mater. 274 (1999) 299.
[4] K. Fukuya, S. Shima, A. Jacobs, G. Wozadlo, S. Suzuki, in: 6th International Conference on Environmental Degradation of Materials in NPS-Water Reactor, TMS, 1993, p. 565.

[5] X.Q. Li, A. Al Mazouzi, Stacking Fault Energy Determination, SCK·CEN Report R-4331, 2007.
[6] Xiaoqiang Li, S. Van Dyck, A. Al Mazouzi, Effect of SFE on Defect Accumulation in Stainless Steels, SCK·CEN Report R-4546, 2007.
[7] M.L. Jenkins, M.A. Kirk, Characterization of Radiation Damage by TEM, IOP Publishing Ltd, 2001.
[8] A.W. Ruff, Met. Trans. 1 (1970) 2392.
[9] Cha Y. Lim, Young G. Kim, Mater. Sci. Eng. A 141 (1991) 67.
[10] T.S. Byun, N. Hashimoto, K. Farrell, Acta. Mater. 52 (2004) 3889.
[11] Xiaoqiang Li, W. Van Renterghem, A. Al Mazouzi, Deformation Mechanisms and Deformation Map Building of Stainless Steel, SCK·CEN Report R-4332, 2007.
[12] L. Bracke, G. Mertens, J. Penning, B.C. De Cooman, Met. Trans. 37 (2006) 307.